





Fluctuations and correlations of reactive scalars near chemical equilibrium in incompressible turbulence

Wenwei Wu (吴文伟) ^{1,2,3,*} Enrico Calzavarini ¹
François G. Schmitt ² and Lipo Wang (王利坡) ³

¹Université de Lille, ULR 7512-Unité de Mécanique de Lille-Joseph Boussinesq (UML), F-59000 Lille, France

²CNRS, Université de Lille, ULCO, Laboratory of Oceanology and Geosciences,
UMR 8187 LOG, Wimereux, France

³UM-SJTU Joint Institute, Shanghai Jiao Tong University, 200240 Shanghai, China



(Received 23 March 2020; accepted 29 July 2020; published 21 August 2020)

The statistical properties of species undergoing chemical reactions in a turbulent environment are studied. We focus on the case of reversible multicomponent reactions of second and higher orders, in a condition close to chemical equilibrium sustained by random large-scale reactant sources, while the turbulent flow is highly developed. In such a state a competition exists between the chemical reaction that tends to dump reactant concentration fluctuations and enhance their correlation intensity and the turbulent mixing that on the contrary increases fluctuations and removes relative correlations. We show that a unique control parameter, the Damköhler number (Da_ϕ), which can be constructed from the scalar Taylor microscale, the reactant diffusivity, and the reaction rate, characterizes the functional dependence of fluctuations and correlations in a variety of conditions, i.e., at changing the reaction order, and the Reynolds and Schmidt numbers. The larger is such a Damköhler number the more depleted are the scalar fluctuations as compared to the fluctuations of a passive scalar field in the same conditions, and vice versa the more intense are the correlations. A saturation in this behavior is observed beyond $Da_\phi \simeq O(10)$. We provide an analytical prediction for this phenomenon which is in excellent agreement with direct numerical simulation results.

DOI: [10.1103/PhysRevFluids.5.084608](https://doi.org/10.1103/PhysRevFluids.5.084608)

I. INTRODUCTION

Turbulence is a ubiquitous complex phenomenon, found in many applied situations such as the automotive industries, chemical engineering, and the environment, including meteorology, oceanography, and even astrophysics. In fully developed turbulence, universal scaling relations are classically discussed in the framework of Kolmogorov-Obukhov phenomenology for the velocity field, as well as the Obukhov-Corrsin approach for passive scalars advected by the turbulent velocity. This now forms the classical Kolmogorov-Obukhov-Corrsin (KOC) theoretical framework for fluid turbulence with advected passive scalars [1].

Chemical reactions have been considered quite early in such a framework, for some specific cases. For example, Corrsin [2] studied the mixing of a scalar contaminant undergoing a first-order chemical reaction in isotropic turbulence. Theoretically he deduced the power spectrum of the reactive scalar in different wave number ranges. Later, Pao [3] investigated the dilute turbulent concentration fields of a multicomponent mixture with first-order reaction and proposed a unified spectral transfer concept for deducing the scalar spectrum at large wave numbers. For higher-order

*wenwei.wu@etu.univ-littoral.fr

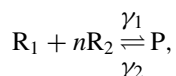
reactions, nonlinearity from the chemical source has also been introduced: O'Brien [4,5] worked on decaying second-order, isothermal reaction in turbulence. The asymptotic decay rate of the scalar energy was found as $t^{-11/2}$ for moderate reactions, and $t^{-3/2}$ for rapid reactions. The covariance between reactants and the development of models for the covariance terms were important topics of turbulent mixing analyses as well [6,7]. For the two non-premixed-reactants case, it was found [8] that the covariance is almost invariant for very slow and very rapid second-order reactions.

Most recent work on such topics have been done for fast reactions and combustion as an application field. Here we mostly focus on higher-order reactions, with possible applications in the field of chemical and biological oceanography, where the typical times of biogeochemical reactions may be large. In such context, some results on the phytoplankton statistics, considered via the proxy of fluorescence measurements, have found some scaling relations with -1.2 spectral slopes, interpreted as a signature of biological activity [9–11]. This generated our motivation here to study the statistical properties of various high-order reactions in a turbulent flow.

In the present work we focus on the fundamental properties of reactive scalar mixing in incompressible turbulence. The flow statistics, from global to scale-dependent features, are studied in detail and theoretically modeled. The article is organized as follows: In Sec. II, we introduce the model system and its governing equations together with the set of dimensionless control parameters. Section III briefly details the numerical methods adopted in this study. The results and their analyses are described in Sec. IV. Finally, Sec. V summarizes the main findings, discussing their implications and future perspectives. In the Appendixes, we provide detailed analytical arguments for the relation between the correlation spectrum of reactive scalar fields and their gradient spectrum, as well as the analytical derivations for the prediction of global reactive scalar correlations and variances.

II. PROBLEM DEFINITION

In this study we consider reactions of the form



where R_1 , R_2 , and P denote three generic reactive scalars and n is an integer coefficient. The process is reversible with independent nonzero forward and backward reaction rates γ_1 and γ_2 . The order of the chemical reaction, which is defined as the sum of the powers of the reactants' concentration in the rate equation, is $n + 1$ for the forward reaction, because the rate equation reads $\gamma_1 R_1 R_2^n$, while it is of the first order for the backward reaction with reaction rate $\gamma_2 P$.

The evolution equations for the concentration fields $R_1(\mathbf{x}, t)$, $R_2(\mathbf{x}, t)$, and $P(\mathbf{x}, t)$ read

$$\partial_t \mathbf{u} + (\mathbf{u} \cdot \nabla) \mathbf{u} = \nu \Delta \mathbf{u} - \nabla p / \rho + \mathbf{f}, \quad (1)$$

$$\nabla \cdot \mathbf{u} = 0, \quad (2)$$

$$\partial_t R_1 + (\mathbf{u} \cdot \nabla) R_1 = D \Delta R_1 - \gamma_1 R_1 R_2^n + \gamma_2 P + \dot{q}_{R_1}, \quad (3)$$

$$\partial_t R_2 + (\mathbf{u} \cdot \nabla) R_2 = D \Delta R_2 - n(\gamma_1 R_1 R_2^n - \gamma_2 P) + \dot{q}_{R_2}, \quad (4)$$

$$\partial_t P + (\mathbf{u} \cdot \nabla) P = D \Delta P + \gamma_1 R_1 R_2^n - \gamma_2 P + \dot{q}_P. \quad (5)$$

Here $\mathbf{u}(\mathbf{x}, t)$ is an incompressible three-dimensional flow velocity described by the Navier-Stokes equations (1) and (2), p is the pressure, ρ is the fluid density set as a constant, ν is the kinematic viscosity, and D is the species diffusivity (assumed as being the same for all species). To sustain the turbulent fluctuations, large-scale forcing terms \mathbf{f} and \dot{q} are introduced for the velocity and scalars, respectively. More details about the expression of these forcing terms are provided in Sec. III.

For comparison, a nonreactive species T undergoing both advection and diffusion is also considered in this study. Its local concentration evolves according to the following equation:

$$\partial_t T + (\mathbf{u} \cdot \nabla) T = D \Delta T + \dot{q}_T. \quad (6)$$

The equations for the above model system can be made dimensionless by choosing reference scales appropriate for the present system. Since the turbulent flow is unbounded, we take the Taylor microscale (λ) and the single component velocity fluctuation (u') as the reference scales for space and velocity, respectively, which are defined as $\lambda = \sqrt{\frac{15\nu}{\varepsilon}} u'$, $u' = \frac{1}{3} \sum_i \sqrt{\langle u_i^2 \rangle}$, and $\varepsilon = \frac{\nu}{2} \langle \sum_i \sum_j (\partial_i u_j + \partial_j u_i)^2 \rangle$. Here ε is the mean dissipation rate and $\langle \dots \rangle$ denotes the space and time (or equivalently ensemble) average. The scalar quantities can be nondimensionalized by means of their equilibrium values in no-flow conditions, $R_{1,eq}$, $R_{2,eq}$, P_{eq} , while for the passive scalar the global mean $\langle T \rangle$ is used as the reference value. Note that at the equilibrium, the algebraic relation $\gamma_1 R_{1,eq} R_{2,eq}^n = \gamma_2 P_{eq}$ holds. Furthermore, in the present work for simplicity we assume that $R_{1,eq} = R_{2,eq}$. This leads to the following dimensionless equations:

$$\partial_t \mathbf{u} + (\mathbf{u} \cdot \nabla) \mathbf{u} = \text{Re}_\lambda^{-1} \Delta \mathbf{u} - \nabla p + \mathbf{f}, \quad (7)$$

$$\nabla \cdot \mathbf{u} = 0, \quad (8)$$

$$\partial_t R_1 + (\mathbf{u} \cdot \nabla) R_1 = (\text{Sc Re}_\lambda)^{-1} \Delta R_1 - \text{Da} (R_1 R_2^n - P) + \dot{q}_{R_1}, \quad (9)$$

$$\partial_t R_2 + (\mathbf{u} \cdot \nabla) R_2 = (\text{Sc Re}_\lambda)^{-1} \Delta R_2 - n \text{Da} (R_1 R_2^n - P) + \dot{q}_{R_2}, \quad (10)$$

$$\partial_t P + (\mathbf{u} \cdot \nabla) P = (\text{Sc Re}_\lambda)^{-1} \Delta P + \text{Da} (R_1 R_2^n - P) + \dot{q}_P, \quad (11)$$

$$\partial_t T + (\mathbf{u} \cdot \nabla) T = (\text{Sc Re}_\lambda)^{-1} \Delta T + \dot{q}_T, \quad (12)$$

where $\text{Re}_\lambda = \lambda u' / \nu$ is the Taylor-based Reynolds number, the Schmidt number $\text{Sc} = \nu / D$ is the ratio of viscous diffusion to molecular diffusion, and the Damköhler number $\text{Da} = \lambda \gamma_1 R_{2,eq}^n / u' = \lambda \gamma_2 / u'$ represents the ratio of flow timescale to the chemical timescale of forward or backward reaction. Note that the particular choice $R_{1,eq} = R_{2,eq}$ is crucial in obtaining a single Damköhler number, instead of two distinct ones that would be present in general cases.

In conclusion the control parameters of the model system are Re_λ , Sc , n , and Da .

III. NUMERICAL METHODS

The model system presented in Sec. II is numerically simulated in a cubic triperiodic domain. The flow is sustained by a large-scale forcing capable to generate a statistically steady homogeneous and isotropic turbulent flow. The expression of the forcing field in Fourier space, $\hat{\mathbf{f}}(\mathbf{k}, t)$, reads

$$\hat{\mathbf{f}}(\mathbf{k}, t) = \frac{1}{\tau_f} \sum_{1 \leq |\mathbf{k}| \leq 2\sqrt{2}} \hat{\mathbf{u}}(\mathbf{k}, t), \quad (13)$$

with τ_f a time scale being adjusted at each time step in order to provide a constant power input, i.e., $\int_V \mathbf{f} \cdot \mathbf{u} dx^3 = \text{const}$. This type of forcing, called linear, has been adopted, e.g., in Ref. [12]. Note also that the zero mode $|\mathbf{k}| = 0$ is not forced in order to prevent the development of a global mean flow; i.e., in our simulations $\langle \mathbf{u} \rangle = 0$. Similarly, the external source term on scalars [\dot{q}_θ with $\theta = R_1, R_2, P$, or T in Eqs. (9)–(12)] is also isotropic and acting at the largest scales; however, it is constant in amplitude [13–15]. In Fourier space this reads

$$\hat{q}_\theta(t) = \sum_{1 \leq |\mathbf{k}| \leq 2\sqrt{2}} \frac{Q}{|\mathbf{k}|} e^{i\phi_\theta(\mathbf{k}, t)}, \quad (14)$$

TABLE I. Parameters for the simulations: Re_λ is the Taylor-scale-based Reynolds number; Sc is the Schmidt number; $\text{Da} = \lambda\gamma_1 R_{2,eq}^n / u' = \lambda\gamma_2 / u'$ is the Damköhler number based on the Taylor scale; n is the order of R_2 in the reaction; N^3 is the total number of grid points; η is the Kolmogorov length or dissipative length; $|\mathbf{k}|_{\max}$ is the maximum wave number amplitude kept by the dealiasing procedure; $|\mathbf{k}|_{\max} \cdot \eta$ is the spatial resolution condition; and dt/τ_η is the time step normalized by the Kolmogorov time scale τ_η .

No.	1	2	3	4
Re_λ	20	40	80	150
Sc	0.1–4	0.1–4	0.1–1/2–4	1
Da	0.0005–50	0.0003–30	0.0005–20	0.001–10
n	1	1–3	1–3	1–3
N^3	64^3	$64^{3a}/128^{3b}$	$128^{3a}/256^{3b}$	256^3
$ \mathbf{k} _{\max}\eta$	3.12	$1.48^a/2.95^b$	$1.26^a/2.52^b$	1.05
dt/τ_η	0.044	$0.06^a/0.03^b$	$0.044^a/0.022^b$	0.034

^aCorresponds to Sc of 0.1–1.

^bCorresponds to Sc of 2–4, better resolution condition is required to resolve the Batchelor microscale ($\frac{\eta}{\text{Sc}^{1/2}}$).

where Q is the constant prescribing the overall source amplitude, and $|k|^{-1}$ is a normalization factor to guarantee that the forcing amplitude is larger at small wave numbers. In particular, the random phase function $\phi_\theta(\mathbf{k}, t)$ is generated independently for each scalar field and δ -correlated both in time and in wave vector [14,15]. As a result, \dot{q}_{R_1} , \dot{q}_{R_2} , \dot{q}_P , and \dot{q}_T have amplitudes of the same order, but they are statistically independent from each other both in time and in space. The set of dynamical equations (7)–(12) is solved numerically by means of a pseudospectral code [16,17] using a smooth dealiasing technique for the treatment of nonlinear terms in the equations [18]. Compared with the conventional 2/3 rule approach, such smooth dealiasing is capable to reduce numerical high-frequency instabilities. The time-marching scheme adopts a third-order Runge-Kutta method.

We explore the parameter space of the problem by means of a series of simulations: the Reynolds number Re_λ varies in the range $\text{Re}_\lambda \in [20, 150]$, the Schmidt number spans the interval [0.1,4], and the Damköhler number changes from $O(10^{-4})$ to $O(10)$, while n is increased from 1 up to $n = 3$ (i.e., from second- to fourth-order forward reaction). The values of the key parameters for the simulations are reported in Table I.

IV. ANALYSIS OF NUMERICAL RESULTS

We begin by looking at the temporal evolution of the two first statistical moments of reactive fields, i.e., their mean values and root-mean-square fluctuations. The notation $\theta = \langle \theta \rangle_V + \theta'$ represents the decomposition into the mean $\langle \cdot \rangle_V$ (volume average) and fluctuation, where θ stands for a generic scalar quantity, either R_1 , R_2 , P , or T .

Figure 1 shows the typical temporal evolution of the fluctuating and the mean parts of scalars for a simulation with $n = 2$, $\text{Da} = 0.1$, $\text{Sc} = 1$, and $\text{Re}_\lambda = 150$. After a sufficiently long simulation time, a statistically steady state is established where the global mean value for the reactive scalar fields is close to the respective equilibrium quantities, i.e., $\langle R_1 \rangle \approx \langle R_2 \rangle \approx \langle P \rangle \approx 1$. Furthermore, in spite of the presence of a vigorous external mechanical forcing and random scalar source terms, the reactive scalar dynamics is characterized by relatively small global fluctuations from the equilibrium state. We observe that the scalar fluctuations are proportional to the amplitude of the mechanical forcing, which poses a limitation for the numerical implementation of the model system, i.e., the positiveness of the scalar concentration fields ($\theta \geq 0$). In order to fulfill this constraint, in this study the rms of scalars reaches at maximum 10% of the mean value. The statistical convergence of our study is reached by means of simulations extending in time $\sim 45T_I$, where $T_I = k/\varepsilon$ with $k = 3u^2/2$ is the integral time scale. The temporal averages are performed after at least $8T_I$ from the beginning of the simulation [see Fig. 1(a)].

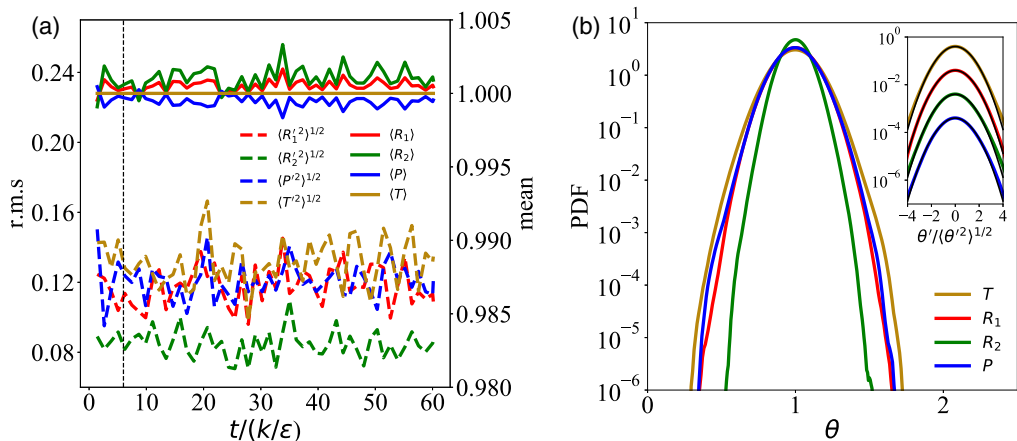


FIG. 1. (a) Evolution of the root mean square of scalar fluctuations and mean values for the case of $n = 2$, $Da = 0.1$, $Sc = 1$, and $Re_\lambda = 150$. Time is normalized by the integral time k/ε with $k = 3u^2/2$. The dashed vertical line marks the initial time for the computation of statistical quantities in this study. (b) PDF of scalar fields in dimensionless units (main panel) and normalized with respect to their standard deviations (inset, the black lines are Gaussian curves). For clarity of visualization, these curves are artificially shifted.

The corresponding probability density functions (PDFs) of the scalar fields are reported in Fig. 1(b). It can be seen that, despite the different amplitudes of the standard deviations, their normalized shapes do not deviate significantly from Gaussian. No noticeable difference is observed in the comparison of reactive scalars with the passive one. Furthermore, side-by-side visualizations of instantaneous snapshots of reactive and passive scalars do not allow to perceive a clear difference in their spatial structure. This leads us to argue that in the present conditions the differences between reactive and passive scalars are to be found in their global properties, such as correlation coefficients and global mean fluctuations, which is the subject of the coming sections.

We also note that in the above described statistically steady condition the advecting flow is the main mechanism responsible for local departures in time and space from the chemical equilibrium condition. The magnitude of such deviations depends on the turbulent intensity and it grows with Re_λ . We observe that the root-mean-square intensity of the local reaction rate $Da(R_1R_2^n - P)$ scales approximately as $\sim Re_\lambda^{3/2}$ in the range of Reynolds number explored in this study.

A. Global correlation coefficients of reactive scalars

In this section the global correlation coefficients for the scalar fields are investigated. We begin with a theoretical argument for the prediction of their functional dependence on varying the dimensionless *a priori* control parameters Re_λ , Sc , Da , and n . We later compare the prediction with the numerical results.

The global correlation coefficients between reactive scalars are defined as

$$r(\theta_1, \theta_2) = \frac{\langle \theta'_1 \theta'_2 \rangle}{\langle \theta_1'^2 \rangle^{1/2} \langle \theta_2'^2 \rangle^{1/2}}, \quad (15)$$

where θ_1 and θ_2 are the scalar fields under consideration.

The theoretical prediction is based on the following two hypotheses. First, given the fact that the reactive scalar fluctuations are small with respect to the equilibrium global value, the chemical sources can be linearized in the following way:

$$R_1R_2^n - P \approx (\langle R_1 \rangle + R'_1)(\langle R_2 \rangle + n\langle R_2 \rangle^{n-1}R'_2) - (\langle P \rangle + P') \approx R'_1 + nR'_2 - P', \quad (16)$$

where we have used also the fact that $\langle R_1 \rangle \approx \langle R_2 \rangle \approx \langle P \rangle \approx 1$ [see again Fig. 1(a)]. Second, we assume that there are no correlations between the source term for a given scalar and other reactive scalars, which is here reasonably guaranteed by the fact that the source terms are δ -correlated in time with a fixed amplitude. Such an assumption, however, is not a general feature of reactive turbulence, and needs to be considered specifically.

The global value of the cross product of scalar gradients $\langle \nabla\theta_1 \nabla\theta_2 \rangle$ can be estimated in terms of the global value of the cross product of scalars $\langle \theta_1 \theta_2 \rangle$ normalized by the square of a characteristic length scale λ_θ . For a scalar quantity θ , we define λ_θ as in Ref. [19]:

$$\lambda_\theta^2 = \frac{\langle \theta'^2 \rangle}{\langle (\partial_x \theta)^2 \rangle}. \quad (17)$$

Such a length can be interpreted as the Taylor microscale of θ (see also Appendix D). Consequently, this allows to introduce an *a posteriori* control parameter, the Damköhler number based on the scalar Taylor microscale and diffusivity, denoted here Da_θ , which is defined as

$$\text{Da}_\theta = \text{Re}_\lambda \text{ScDa} \lambda_\theta^2 = \frac{\lambda_\theta^2}{D} \gamma_1 R_{2,eq}^n. \quad (18)$$

It has to be noted that such a number includes a combination of the three *a priori* control parameters (Re_λ , Sc , and Da) for the model system, with the addition of the λ_θ scale, which therefore plays a key role in the analysis.

We provide here the central result of the derivation based on the above steps. The detailed derivation, lengthy but straightforward, is provided in Appendix A. It is found that $r(R_1, R_2)$, $r(R_1, P)$, and $r(R_2, P)$ are only dependent on the reaction order n and Da_θ . Specifically,

$$r(R_1, P) \approx \frac{\text{Da}_\theta}{3 + n^2 \text{Da}_\theta + \text{Da}_\theta}, \quad (19)$$

$$r(R_1, R_2) = -r(R_2, P) \approx \frac{-n \text{Da}_\theta}{\sqrt{3 + n^2 \text{Da}_\theta + \text{Da}_\theta} \sqrt{3 + 2 \text{Da}_\theta}}. \quad (20)$$

The above expressions show that the concentration field for R_1 is positively correlated to P , while it is negatively correlated to R_2 . Furthermore, the correlations $r(R_1, R_2)$ and $r(R_2, P)$ are opposite in sign. They also show that for large Da_θ the correlations reach a saturation plateau, whose value depends on the reaction order n . For $n = 1$ the correlation coefficients all have the same intensity and only differ in sign. The asymptotically large Da_θ limit in this case leads to the values $r = \pm 1/2$. At asymptotically large n and Da_θ , it yields $r(R_1, P) \simeq 0$ and $r(R_1, R_2) = -r(R_2, P) \simeq 1$. On the contrary, in the condition of vanishing values of Da_θ , corresponding to a negligible role of chemical processes and predominance of mixing, all the correlation coefficients tend to zero.

In Fig. 2 we report the numerical measurements of the correlation coefficients between the reactive scalars as functions of Da_θ , for a set of simulations characterized by different reaction order n and different Re_λ , ranging over more than a decade. It can be seen that for low Da_θ values, corresponding to slow reaction rates, R_1 , R_2 , and P behave as almost independent passive scalars, as expected. Thus the correlation coefficients are about zero when Da_θ is small. As Da_θ increases, the scalars become more and more correlated and the correlation coefficients gradually approach plateaus, which are n dependent. All these tendencies are in excellent agreement with the theoretical predictions, which are also reported in the same figure.

Figure 3 further confirms the range of validity of the prediction, by displaying the same correlations now for the case of different Schmidt numbers in the range from 0.1 to 4 and for $n = 1$. Again the trends are well captured by the theoretical predictions.

B. Variance of reactant scalar fields as compared to a passive scalar

As we have already mentioned, the turbulent advection and the scalar forcing are the sources of scalar spatial-temporal fluctuations. In the case of passive scalars such fluctuations are smoothed

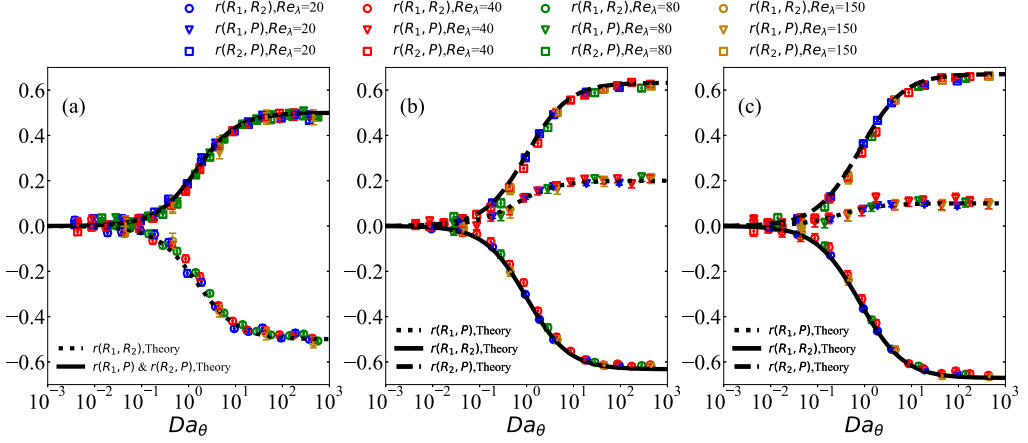


FIG. 2. Correlation coefficients between R_1 and R_2 ($r(R_1, R_2)$), R_1 and P ($r(R_1, P)$), R_2 and P ($r(R_2, P)$) as functions of Da_θ , under the conditions of (a) $n = 1$ (b) $n = 2$, and (c) $n = 3$ and the Schmidt number $Sc = 1$. Theoretical predictions are shown as black lines.

out by diffusion. For the reactive case, the chemical sources function as an additional dumping mechanism. In other words, it is expected that the chemical reaction term acts as a global sink to suppress the scalar energy to dissipation via molecular diffusion.

In the present model system this scenario can be understood by means of the following argument. We multiply the linearized transport equations for the reactive scalars [Eqs. (A2)–(A4) in Appendix A] with the corresponding fluctuation field R'_1 , R'_2 , and P' and perform volume and time averaging $\langle \cdot \rangle$. At a statistical stationary state, summing the obtained equations of scalar dissipation rates (ε_{R_1} , ε_{R_2} , and ε_P) for the considered reactive fields reads

$$\begin{aligned} \varepsilon_{R_1} + \varepsilon_{R_2} + \varepsilon_P &= \frac{\langle (\nabla R'_1)^2 \rangle}{Re_\lambda Sc} + \frac{\langle (\nabla R'_2)^2 \rangle}{Re_\lambda Sc} + \frac{\langle (\nabla P')^2 \rangle}{Re_\lambda Sc} \\ &\approx -Da \langle R'_1 + nR'_2 - P' \rangle^2 + \langle R'_1 \dot{q}_{R_1} \rangle + \langle R'_2 \dot{q}_{R_2} \rangle + \langle P' \dot{q}_P \rangle. \end{aligned} \quad (21)$$

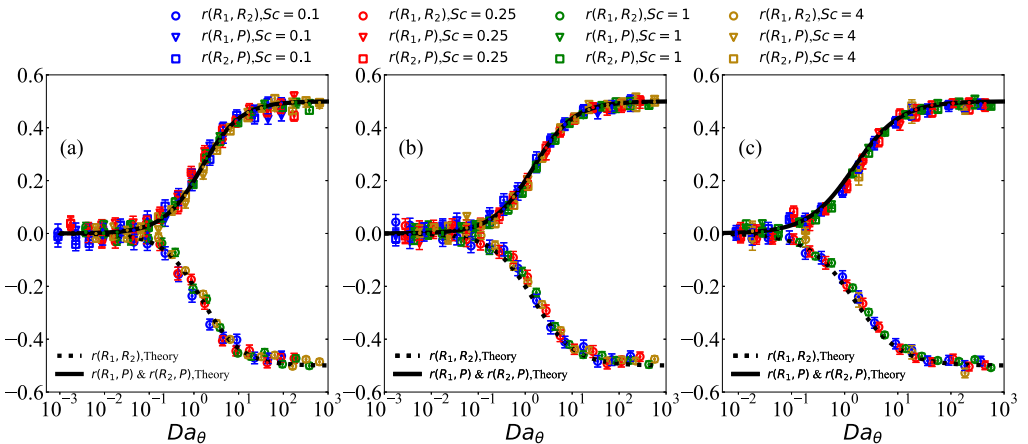


FIG. 3. Correlation coefficients between R_1 and R_2 ($r(R_1, R_2)$), R_1 and P ($r(R_1, P)$), R_2 and P ($r(R_2, P)$) as functions of Da_θ , under the conditions of (a) $Re_\lambda = 20$, (b) $Re_\lambda = 40$, and (c) $Re_\lambda = 80$. The order of R_2 (n) is 1. Theoretical predictions are shown as black lines.

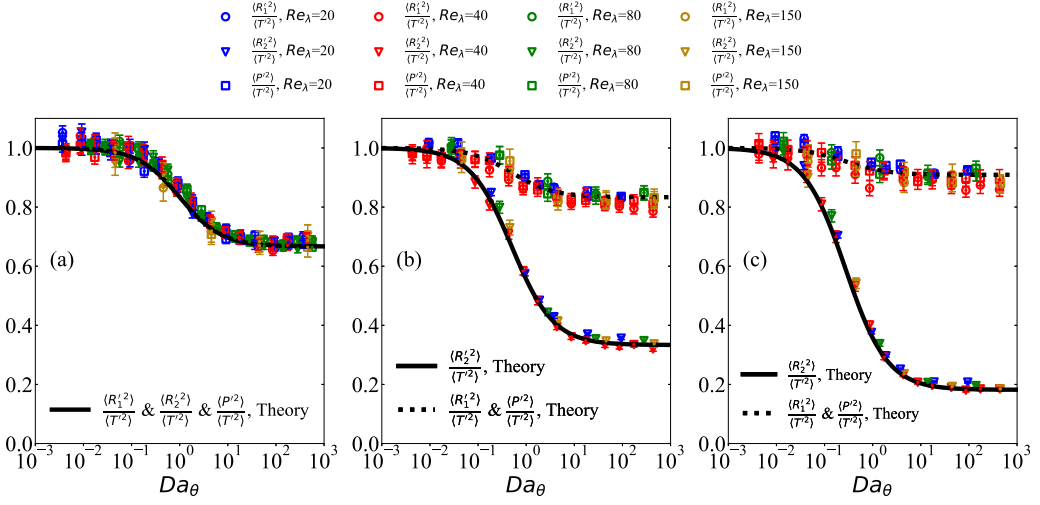


FIG. 4. The fluctuations of the reactive scalars normalized by the fluctuation of the passive scalar (T) as functions of Da_θ , under the conditions of (a) $n = 1$, (b) $n = 2$, and (c) $n = 3$, and the Schmidt number $Sc = 1$. Theoretical predictions are shown as black lines.

The above equation shows that the reaction is always responsible for removing the scalar energy. A consequence of this is that one expects smaller scalar fluctuations for the reactive fields as compared to a passive scalar. In particular, we expect that the scalar variance will be a monotonically decreasing function of Da_θ .

To have a quantitative understanding of such a scenario we compare the fluctuations of the reactive scalars with the ones of a passive scalar in the same dynamical conditions, i.e., subject to the same advective flow, and having the same diffusion and under the effect of an independent statistical realisation of the source term \dot{q}_θ .

In order to develop also in this case a quantitative prediction for the phenomenon, we need to introduce the key assumption that the scalar energy input due to the source term on the field R_1 is approximately same as the one provided on a passive scalar field T in the same conditions, i.e.,

$$\langle R_1' \dot{q}_{R_1} \rangle \simeq \langle T' \dot{q}_T \rangle. \quad (22)$$

The soundness of this hypothesis lies in the fact that in the present conditions the reactant R_1 has a fluctuation of similar intensity as the passive scalar case.

Following a similar derivation as for Eqs. (19) and (20), the fluctuations of the reactive scalars normalized by the fluctuation of the passive scalar (T) are estimated as

$$\frac{\langle R_2^2 \rangle}{\langle T^2 \rangle} \approx \frac{3 + 2Da_\theta}{3 + n^2 Da_\theta + 2Da_\theta}, \quad (23)$$

$$\frac{\langle R_1^2 \rangle}{\langle T^2 \rangle} = \frac{\langle P^2 \rangle}{\langle T^2 \rangle} \approx \frac{3 + n^2 Da_\theta + Da_\theta}{3 + n^2 Da_\theta + 2Da_\theta}. \quad (24)$$

For the full details for this derivation, which implies performing spatial and temporal averaging over the scalar energy equations, the reader is referred to Appendix B. It is found that the fluctuations of the reactive scalars (R_1 , R_2 , and P) are close to that of the passive scalar (T) when Da_θ is small, but gradually decrease as Da_θ increases. Figure 4 shows the normalized fluctuations of the reactive scalars (R_1 , R_2 , and P) as measured from the direct numerical simulation, in agreement with the above theoretical prediction.

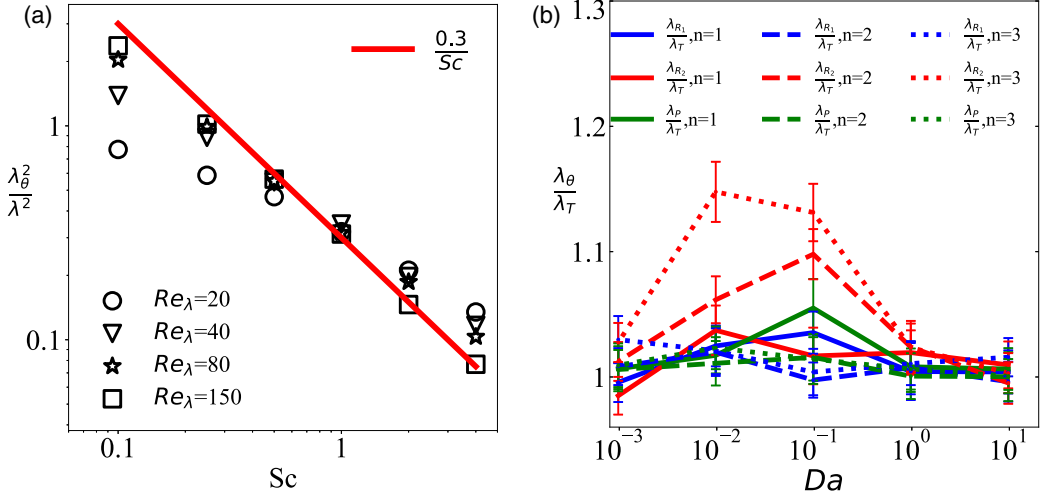


FIG. 5. (a) Taylor microscales of scalars (computed on T) as functions of Sc . The red line is $0.3/St$. A power law fit of the form aSc^b on the $Re_\lambda = 150$ data set gives $a = 0.29 \pm 0.1$ and $b = -0.93 \pm 0.02$. (b) Taylor microscales of the reactive scalars with respect to the passive scalar with different orders of reaction, as functions of Da for all the simulations at $Re_\lambda = 150$ and $Sc = 1$.

C. On the Taylor microscale of scalar concentration fields

As we have discussed in the above sections the correlations and fluctuations of the concentration of reactive scalars are well described by means of the control parameter Da_θ , which contains the scalar Taylor microscale of λ_θ . In this section we aim at gaining more insight into this key spatial scale.

The scalar Taylor microscale was notably first studied by Corrsin [20], in the context of scalar mixing in turbulent flows. He hypothesized that such a scale is proportional to the intensity of turbulence and inversely to the Schmidt number of the problem, i.e.,

$$\frac{\lambda_\theta^2}{\lambda^2} \propto \frac{1}{Sc}.$$

However, further experimental and numerical studies [21,22] have reported that such a dependence is not straightforward, as it shows finite Re_λ effects and different trends for asymptotically small and large Sc values (see [19] for a recent discussion).

We show the results of our simulations in Fig. 5(a). The figure reports the dimensionless λ_θ^2 (actually $\lambda_\theta^2/\lambda^2$, because the length is nondimensionalized by λ) as functions of Sc under the conditions of Re_λ from 20 to 150. Figure 5 indicates that a clear -1 scaling law exists between λ_θ^2 and Sc for the largest Re_λ case, with a prefactor $\simeq 0.3$, implying that in the limit of intense turbulence Da_θ can be approximated as

$$Da_\theta \simeq 0.3Re_\lambda Da = 3T_I/\tau_r. \quad (25)$$

Here $\tau_r = (\gamma_1 R_{2,eq})^{-1}$ is the typical time of the reaction. Remarkably, this result reveals that the unique *a posteriori* control parameter that we have identified with Da_θ can be considered as the ratio of the largest time scale of the turbulent flow to the typical time scale associated to the chemical process.

Finally, we remark that λ_θ does not vary significantly over the different scalar fields R_1 , R_2 , and P and the reference passive scalar field T . This is exemplified in Fig. 5(b) for all the simulations at $Re_\lambda = 150$ and $Sc = 1$. The figure shows that any λ_θ evaluated on a reactive field is at most 15% different from the reference λ_T case. Such a difference vanishes for very small (the mixing

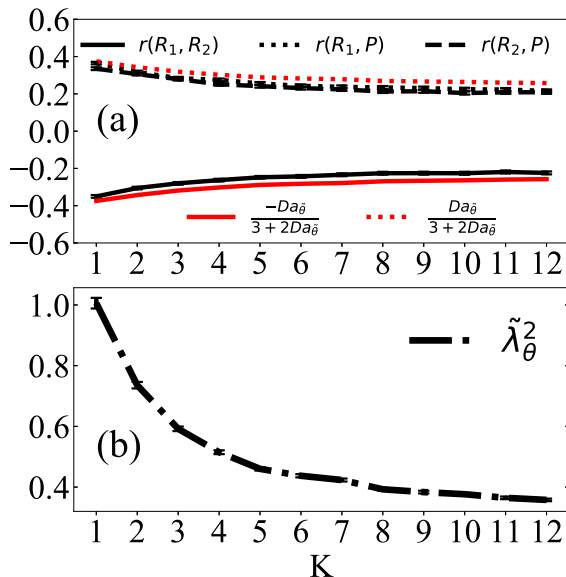


FIG. 6. (a) Correlation coefficients of scalar evolving in a coarse-grained turbulent flow field, compared with theoretical predictions, and (b) Taylor microscales of the scalars convected by filtered velocity ($\tilde{\lambda}_\theta$) as functions of the maximum wave number of filtered velocity (K), at $Sc = 1$, $Re_\lambda = 80$, and $Da = 0.05$ ($Da_\theta = 1.42$).

dominated limit) or very large Da and shows a weak increase trend with the order of the reaction. We can conclude that λ_T can here be taken as a convenient approximation of λ_θ . The estimations of Da_θ in the present work are based on such an assumption.

Taylor microscale of scalars advected by a coarse-grained turbulent flow field

In order to understand better the role of λ_θ , we perform a series of simulations where the scalar fields are advected by a coarse-grained, i.e., spatially filtered, turbulent flow, denoted as $\tilde{\mathbf{u}}$. The filter is a spectral low pass, defined as

$$\hat{\mathbf{u}} = \sum_{|\mathbf{k}| \leq K} \hat{\mathbf{u}}(\mathbf{k}), \quad (26)$$

where K specifies the maximum wave number kept in the modified field. Such a filter retains only the large eddies of the turbulent flow, down to a wavelength $2\pi/K$. The Taylor scale for scalars convected by the filtered flow is denoted as $\tilde{\lambda}_\theta$. It is noteworthy that the length quantities are always adimensionalized by the Taylor scale of unfiltered flow λ , instead of the Taylor scale of the filtered flow. It is worth exploring what is the impact of the hierarchy of flow scales, extending from the domain size down to the dissipative scales, on the reactive scalar dynamics. In particular, we aim at understanding the dependence of the scalar correlation coefficients and the scalar Taylor microscale on the maximum wave number K . According to the above discussion, it is reasonably expected that the small scales of the fluid have a negligible influence, because the scaling mixing process and relevant quantities are controlled by the large eddy turnover time T_l .

Results are presented for a typical case, i.e., $Sc = 1$, $Re_\lambda = 80$, and $Da = 0.05$ corresponding to $Da_\theta = 1.42$. Figure 6(a) shows that the correlation coefficients vary quite weakly with the filter parameter K . The deviation becomes noticeable only for $K \leq 3$, which corresponds to scales larger than the large eddy turnover scale of the flow, in the sense that the forcing is active up to $|\mathbf{k}| = 2\sqrt{2}$. Such behavior is also well captured by the theoretical predictions of Eqs. (19) and (20) if

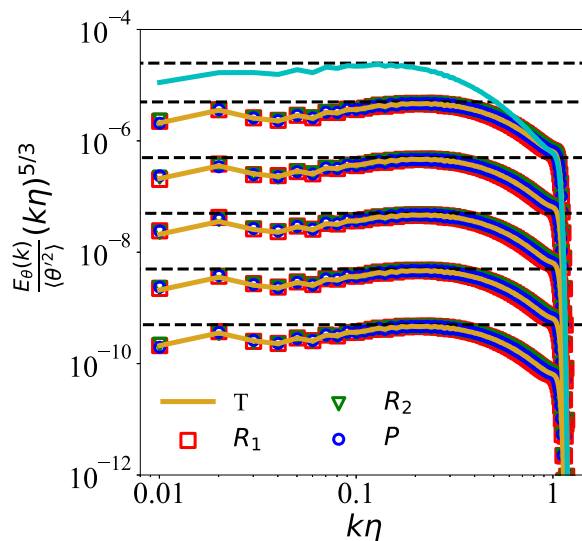


FIG. 7. Energy spectra of reactive and passive scalar fields, i.e., $E_\theta(k)$ with $\theta = R_1, R_2, P$, and T , and velocity field $E_u(k)$ (solid light blue line) in the condition $\text{Re}_\lambda = 150$, $\text{Sc} = 1$, $n = 1$, and $\text{Da} = 10, 1, 0.1, 0.01$, and 0.001 (from top to bottom). Each spectra is compensated with the KOC scaling $(k\eta)^{5/3}$ and normalized by the global energy $\langle \theta^2 \rangle$. For clarity, the energy spectra of scalars are shifted vertically by a multiplicative factor of 0.1.

the Damköhler number $\text{Da}_{\tilde{\lambda}_\theta}$ adopted is built on the measured scalar Taylor scale $\tilde{\lambda}_\theta$, instead of the original Da_θ . This confirms again the relevance of the scalar Taylor microscale in characterizing the present reactive scalar system. Finally we note that, differently from the correlation coefficients, the scale $\tilde{\lambda}_\theta$ varies sensibly with the filter wave number K , as reported in Fig. 6(b).

D. Spectra and coherency spectra of reactive scalars

In this section we focus on the scale-dependent behavior of reactive scalar fluctuations and their mutual correlation.

1. Energy spectrum

The energy spectra of the velocity and scalars are defined as

$$E_u(k) = 4\pi k^2 \left\langle \frac{1}{2} \hat{u}_i(\mathbf{k}) \hat{u}_i^*(\mathbf{k}) \right\rangle_k, \quad (27)$$

$$E_\theta(k) = 4\pi k^2 \langle \hat{\theta}(\mathbf{k}) \hat{\theta}^*(\mathbf{k}) \rangle_k, \quad \theta = R_1, R_2, P, \text{ and } T, \quad (28)$$

where $\langle \cdot \rangle_k$ denotes the average over all the modes in the shell of thickness Δk centered at $k = |\mathbf{k}|$ and time, $\hat{u}_i(\mathbf{k})$ and $\hat{\theta}(\mathbf{k})$ are the Fourier coefficients of the mode of \mathbf{k} , and $\hat{u}_i^*(\mathbf{k})$ and $\hat{\theta}^*(\mathbf{k})$ are the corresponding complex conjugate fields.

Figure 7 depicts the log-log plots of the three-dimensional energy spectra of scalars of a typical case at $\text{Re}_\lambda = 150$, $\text{Sc} = 1$, and $n = 1$, compensated with $\sim k^{-5/3}$, which is the scaling expected in the inertial regime both for the velocity and for a passive scalar field, i.e., the KOC scaling [23,24]. The spectra are also normalized by the total energy for each scalar. The figure shows that the spectra are indistinguishable from the ones of a passive scalar and display the same scaling in the inertial range. This proves that in the present condition the reaction terms have a negligible effect on the scalar energy transfer. Remarkably, this behavior is also Damköhler number independent. The latter

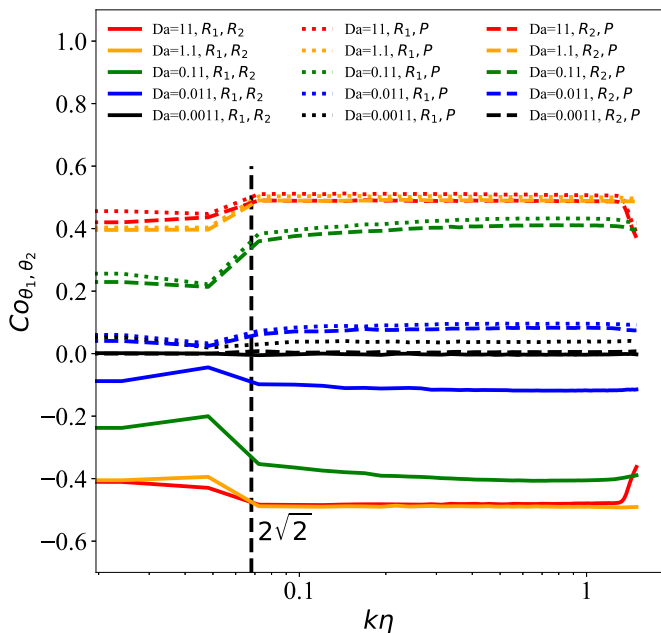


FIG. 8. Coherency spectra of the reactive scalars, under the conditions of $\text{Re}_\lambda = 80$, $\text{Sc} = 1$, and $n = 1$. The horizontal axis is normalized in terms of the Kolmogorov scale η . The dashed vertical line marks the maximum wave number at which the scalar source terms act.

observation is qualitatively confirmed also by visualizations of the instantaneous scalar fields for different Da values. Despite perceptible larger fluctuations for the small- Da case (the one where the chemistry is slower), it appears that the spatial structure of the fields is not affected by the magnitude of Da .

2. Coherency spectra

The coherency spectrum between two scalar fields θ_1 and θ_2 is defined as

$$\text{Co}_{\theta_1, \theta_2}(k) = \frac{\langle |\widehat{\theta}_1(\mathbf{k})\widehat{\theta}_2^*(\mathbf{k})| \rangle_k}{\sqrt{\langle \widehat{\theta}_1(\mathbf{k})\widehat{\theta}_1^*(\mathbf{k}) \rangle_k \langle \widehat{\theta}_2(\mathbf{k})\widehat{\theta}_2^*(\mathbf{k}) \rangle_k}}. \quad (29)$$

This function describes the scale dependence, in spectral space, of the correlation coefficient between two scalar fields. Figure 8 shows the results for a typical case at fixed $\text{Re}_\lambda = 80$, $\text{Sc} = 1$, $n = 1$ and varying Da . It is interesting to note that for all the Da cases the coherency spectra are nearly k independent; in particular, they are constant in the inertial range. A nonconstant behavior is observed at small wave numbers $|\mathbf{k}| \lesssim 2\sqrt{2}$, which correspond to the largest physical scales. This is due to the action of the random scalar source that strongly reduces the intensity of correlations. Moreover, the absolute value of $\text{Co}_{\theta_1, \theta_2}$ increases as Da increases, which agrees with the picture that fast chemical reactions build up correlations.

V. CONCLUSIONS AND OUTLOOK

In summary, the statistical properties of species undergoing reversible chemical reactions in incompressible turbulence have been studied. We have addressed this by means of a model system in which the flow is statistically steady turbulence and the chemical species are retained in a dynamical equilibrium state due to the action of random large-scale source terms. It is observed that the reactive

scalar fluctuations have a Gaussian distribution and energy spectra are essentially identical to the one of a passive scalar field transported by the same flow. This can be explained by the overall small amplitude of the reaction terms in the present close-to-equilibrium condition.

However, in such a state a competition still exists between the chemical processes, which tend to dump reactant concentration fluctuations and enhance their correlation intensity, and the turbulent mixing, which on the contrary increases fluctuations and removes relative correlations.

We quantitatively describe this phenomenon by considering the linearized equations for the reactive scalar fluctuations. A unique control parameter, the Damköhler number (Da_θ), can be constructed as the ratio between the time scale of scalar diffusion across a domain of the size of the scalar Taylor microscale (λ_θ^2/D) and the chemical reaction time scale τ_r . Importantly, Da_θ characterizes the functional dependence of fluctuations and correlations of the scalar quantities in the full range of explored conditions with variable reaction order, the Reynolds number, and the Schmidt number. The larger is such a Damköhler number the more depleted are the scalar fluctuations as compared to the fluctuation of a passive scalar field in the same conditions, and vice versa the more intense are the correlations. A saturation in this behavior is observed beyond $Da_\theta \simeq O(10)$. These results reveal the significance of the scalar Taylor microscale for problems involving the mixing of chemical species. We have shown that in the limit of intense turbulence the relation proposed by Corrsin [20], $\lambda_\theta \sim \lambda Sc^{-1/2}$, holds approximately, meaning that Da_θ can also be viewed as the ratio of the large-eddy-turnover time of the flow over the typical chemical reaction time.

The latter observation can be of practical interest for the estimation of the regimes attained by biogeochemical reactions at small scales in the ocean. For example, one can consider a reactive field as the local concentration of phytoplankton in the ocean. The times scales used to construct Da_θ are the typical large-eddy-turnover time of the three-dimensional turbulent flow, which is normally of the order of hours [25], and the typical growth rate of the population that is on the order of a day. This leads to a value of $Da_\theta < 1$, meaning that, at small scales, more precisely at scales where the oceanic flow can be approximated as a three-dimensional turbulent flow with a direct energy cascade, the phytoplankton concentration can be safely considered as a passive scalar field. However, differently from the situation explored in this work, the fluctuations displayed by planktonic populations can attain values that are comparable to the ones of the mean population density. This means that there exist regions where nearly any individual can be found or where huge accumulation can be observed. These situations go beyond the model explored in this work, and beyond the linearized theoretical predictions that we put forward. For this reason, it will be interesting to explore in the future different flow configurations where strong chemical sources could produce pronounced deviations from the global equilibrium state.

ACKNOWLEDGMENTS

This work is under the joint support of Shanghai Jiao Tong University and French Region ‘‘Hauts-de-France’’ in the framework of a cotutella Ph.D. program. We thank Dr. Michael Gauding (CORIA (CNRS UMR 6614), Rouen, France) for providing the code. We acknowledge the computing resources including the High Performance Computing Center (HPCC) at Université de Lille, CALCULCO of Université du Littoral Côte d’Opale, and the National Supercomputer Center in Guangzhou, China.

APPENDIX A: ANALYTICAL PREDICTION FOR REACTANT CORRELATIONS

Under the conditions of $R'_1 \ll \langle R_1 \rangle$, $R'_2 \ll \langle R_2 \rangle$, $P' \ll \langle P \rangle$, and $\langle R_1 \rangle \approx \langle R_2 \rangle \approx \langle P \rangle \approx 1$ (Fig. 1), the net reaction rate can be estimated as

$$R_1 R_2^n - P \approx (\langle R_1 \rangle + R'_1)(\langle R_2 \rangle + n\langle R_2 \rangle^{n-1} R'_2) - (\langle P \rangle + P') \approx R'_1 + nR'_2 - P'. \quad (A1)$$

Correspondingly, the equations for fluctuating scalars become

$$\frac{DR'_1}{Dt} \approx \frac{1}{\text{Re}_\lambda \text{Sc}} \Delta R'_1 - \text{Da}(R'_1 + nR'_2 + M') + \dot{q}_{R_1}, \quad (\text{A2})$$

$$\frac{DR'_2}{Dt} \approx \frac{1}{\text{Re}_\lambda \text{Sc}} \Delta R'_2 - n\text{Da}(R'_1 + nR'_2 + M') + \dot{q}_{R_2}, \quad (\text{A3})$$

$$\frac{DM'}{Dt} \approx \frac{1}{\text{Re}_\lambda \text{Sc}} \Delta M' - \text{Da}(R'_1 + nR'_2 + M') + \dot{q}_M, \quad (\text{A4})$$

where $M' = -P'$ and $\dot{q}_M = -\dot{q}_P$. The same form of Eq. (A4) as Eq. (A2) implies that R'_1 and M' behave statistically the same.

Multiplying Eqs. (A2)–(A4) with R'_2 , M' , and R'_1 , respectively, and averaging ($\langle \dots \rangle$) on time and space yields

$$\left\langle \frac{DR'_1}{Dt} R'_2 \right\rangle + \frac{1}{\text{Re}_\lambda \text{Sc}} \langle \nabla R'_2 \nabla R'_1 \rangle \approx -\text{Da}(\langle R'_2 R'_1 \rangle + n\langle R_2'^2 \rangle + \langle R'_2 M' \rangle) + \langle R'_2 \dot{q}_{R_1} \rangle, \quad (\text{A5})$$

$$\left\langle \frac{DR'_2}{Dt} M' \right\rangle + \frac{1}{\text{Re}_\lambda \text{Sc}} \langle \nabla M' \nabla R'_2 \rangle \approx -n\text{Da}(\langle M' R'_1 \rangle + n\langle M' R'_2 \rangle + \langle M'^2 \rangle) + \langle M' \dot{q}_{R_2} \rangle, \quad (\text{A6})$$

$$\left\langle \frac{DM'}{Dt} R'_1 \right\rangle + \frac{1}{\text{Re}_\lambda \text{Sc}} \langle \nabla R'_1 \nabla M' \rangle \approx -\text{Da}(\langle R_1'^2 \rangle + n\langle R'_1 R'_2 \rangle + \langle R'_1 M' \rangle) + \langle R'_1 \dot{q}_M \rangle. \quad (\text{A7})$$

In Eq. (A5), the term $\langle R'_2 \dot{q}_{R_1} \rangle$ is estimated as zero, because the time-delta forcing to one scalar (R_1) cannot be strongly correlated with another scalar (R_2). Moreover, the small net reaction rate implies that the instantaneous reactive scalar is weakly influenced by other scalar(s). Thus at the statistical stationary state, $\langle \frac{DR'_1}{Dt} R'_2 \rangle$ can be assumed negligibly small, i.e., $\langle \frac{DR'_1}{Dt} R'_2 \rangle \sim 0$.

As discussed in Appendix D, the correlation coefficients of the reactive scalars are roughly the same as the correlation coefficients of their gradients, which in isotropic turbulence can be estimated as

$$\begin{aligned} \langle \partial_x R'_2 \partial_x R'_1 \rangle &\approx \langle \partial_y R'_2 \partial_y R'_1 \rangle \approx \langle \partial_z R'_2 \partial_z R'_1 \rangle \\ &\approx \langle (\partial_x R'_2)^2 \rangle^{1/2} \langle (\partial_x R'_1)^2 \rangle^{1/2} \frac{\langle R'_2 R'_1 \rangle}{\langle R_2'^2 \rangle^{1/2} \langle R_1'^2 \rangle^{1/2}} \\ &\approx \frac{\langle R_2'^2 \rangle^{1/2} \langle R_1'^2 \rangle^{1/2}}{\lambda_\theta^2} \frac{\langle R'_2 R'_1 \rangle}{\langle R_2'^2 \rangle^{1/2} \langle R_1'^2 \rangle^{1/2}} \approx \frac{\langle R'_2 R'_1 \rangle}{\lambda_\theta^2}, \end{aligned} \quad (\text{A8})$$

where λ_θ is the Taylor microscale for scalars.

Consequently,

$$\frac{1}{\text{Re}_\lambda \text{Sc}} \langle \nabla R'_2 \nabla R'_1 \rangle = \frac{1}{\text{Re}_\lambda \text{Sc}} (\langle \partial_x R'_2 \partial_x R'_1 \rangle + \langle \partial_y R'_2 \partial_y R'_1 \rangle + \langle \partial_z R'_2 \partial_z R'_1 \rangle) \approx \frac{3}{\text{Re}_\lambda \text{Sc} \lambda_\theta^2} \langle R'_2 R'_1 \rangle. \quad (\text{A9})$$

From Eq. (A5) it yields

$$3\langle R'_2 R'_1 \rangle \approx -\text{Da}_\theta (\langle R'_2 R'_1 \rangle + n\langle R_2'^2 \rangle + \langle R'_2 M' \rangle), \quad (\text{A10})$$

where $\text{Da}_\theta = \text{Re}_\lambda \text{Sc} \lambda_\theta^2 \text{Da} = \frac{\lambda_\theta^2 \gamma R_{2,eq}^0}{D}$ is the Damköhler number based on the scalar Taylor microscale and diffusivity.

Similarly, from Eqs. (A6) and (A7),

$$3\langle M' R'_2 \rangle \approx -n\text{Da}_\theta (\langle M' R'_1 \rangle + n\langle M' R'_2 \rangle + \langle M'^2 \rangle), \quad (\text{A11})$$

$$3\langle R'_1 M' \rangle \approx -\text{Da}_\theta (\langle R_1'^2 \rangle + n\langle R'_1 R'_2 \rangle + \langle R'_1 M' \rangle). \quad (\text{A12})$$

Because R'_1 and M' are statistically the same [see Eqs. (A2) and (A4)], we can define

$$C = \langle R'_1 M' \rangle, \quad c = \langle R'_2 R'_1 \rangle = \langle R'_2 M' \rangle, \quad V = \langle R_1'^2 \rangle = \langle M'^2 \rangle, \quad v = \langle R_2'^2 \rangle, \quad (\text{A13})$$

i.e.,

$$\frac{C}{V} = r(R_1, M) = -r(R_1, P), \quad \frac{c}{\sqrt{V}v} = r(R_1, R_2) = r(R_2, M) = -r(R_2, P).$$

Then Eqs. (A10)–(A12) can be rewritten as

$$3c \approx -\text{Da}_\theta(2c + nv), \quad (\text{A14})$$

$$3c \approx -n\text{Da}_\theta(C + nc + V), \quad (\text{A15})$$

$$3C \approx -\text{Da}_\theta(C + nc + V), \quad (\text{A16})$$

which then leads to the solutions of Eqs. (19) and (20) as

$$r(R_1, P) = -\frac{C}{V} \approx \frac{\text{Da}_\theta}{3 + n^2\text{Da}_\theta + \text{Da}_\theta},$$

$$r(R_1, R_2) = -r(R_2, P) = \frac{c}{\sqrt{V}v} \approx \frac{-n\text{Da}_\theta}{\sqrt{3 + n^2\text{Da}_\theta + \text{Da}_\theta}\sqrt{3 + 2\text{Da}_\theta}}.$$

APPENDIX B: ANALYTICAL PREDICTION FOR REACTANT VARIANCES

By multiplying Eqs. (A2)–(A4) with R'_1 , R'_2 , and M' , respectively, and averaging ($\langle \cdot \cdot \rangle$) in space and time, we obtain

$$\frac{1}{2} \frac{D\langle R_1'^2 \rangle}{Dt} + \frac{1}{\text{Re}_\lambda \text{Sc}} \langle |\nabla R_1'|^2 \rangle \approx -\text{Da}(\langle R_1'^2 \rangle + n\langle R_1' R'_2 \rangle + \langle R_1' M' \rangle) + \langle R_1' \dot{q}_{R_1} \rangle, \quad (\text{B1})$$

$$\frac{1}{2} \frac{D\langle R_2'^2 \rangle}{Dt} + \frac{1}{\text{Re}_\lambda \text{Sc}} \langle |\nabla R_2'|^2 \rangle \approx -n\text{Da}(\langle R_1' R'_2 \rangle + n\langle R_2'^2 \rangle + \langle R_2' M' \rangle) + \langle R_2' \dot{q}_{R_2} \rangle, \quad (\text{B2})$$

$$\frac{1}{2} \frac{D\langle M'^2 \rangle}{Dt} + \frac{1}{\text{Re}_\lambda \text{Sc}} \langle |\nabla M'|^2 \rangle \approx -\text{Da}(\langle R_1' M' \rangle + n\langle R_2' M' \rangle + \langle M'^2 \rangle) + \langle M' \dot{q}_M \rangle. \quad (\text{B3})$$

The dissipation terms above, e.g., $\frac{1}{\text{Re}_\lambda \text{Sc}} \langle |\nabla R_1'|^2 \rangle$, can be estimated similarly as Eq. (A8). Under the isotropic and statistical stationary conditions, the turbulent energies of R'_1 , R'_2 , and P' are approximately determined as

$$3\langle R_1'^2 \rangle \approx -\text{Da}_\theta(\langle R_1'^2 \rangle + n\langle R_1' R'_2 \rangle + \langle R_1' M' \rangle) + \text{Re}_\lambda \text{Sc} \lambda_\theta^2 \langle R_1' \dot{q}_{R_1} \rangle, \quad (\text{B4})$$

$$3\langle R_2'^2 \rangle \approx -n\text{Da}_\theta(\langle R_1' R'_2 \rangle + n\langle R_2'^2 \rangle + \langle R_2' M' \rangle) + \text{Re}_\lambda \text{Sc} \lambda_\theta^2 \langle R_2' \dot{q}_{R_2} \rangle, \quad (\text{B5})$$

$$3\langle M'^2 \rangle \approx -\text{Da}_\theta(\langle R_1' M' \rangle + n\langle R_2' M' \rangle + \langle M'^2 \rangle) + \text{Re}_\lambda \text{Sc} \lambda_\theta^2 \langle M' \dot{q}_M \rangle. \quad (\text{B6})$$

Similarly, based on Eq. (12), the turbulent energy of T' is

$$3\langle T'^2 \rangle \approx \text{Re}_\lambda \text{Sc} \lambda_\theta^2 \langle T' \dot{q}_T \rangle. \quad (\text{B7})$$

Define

$$w = \text{Re}_\lambda \text{Sc} \lambda_\theta^2 \langle R_2' \dot{q}_{R_2} \rangle, \quad W = \text{Re}_\lambda \text{Sc} \lambda_\theta^2 \langle R_1' \dot{q}_{R_1} \rangle = \text{Re}_\lambda \text{Sc} \lambda_\theta^2 \langle M' \dot{q}_M \rangle,$$

$$V_T = \langle T'^2 \rangle, \quad W_T = \text{Re}_\lambda \text{Sc} \lambda_\theta^2 \langle T' \dot{q}_T \rangle. \quad (\text{B8})$$

Together with Eqs. (A13), (B4), (B5), and (B7) we obtain

$$3V \approx -\text{Da}_\theta(V + nc + C) + W, \quad (\text{B9})$$

$$3v \approx -n\text{Da}_\theta(2c + v) + w, \quad (\text{B10})$$

$$3V_T \approx W_T. \quad (\text{B11})$$

It is worth noting that for all the scalar quantities the delta-correlated external forcing is exerted in the same way with constant amplitude. When $\langle R_1'^2 \rangle$ is close to $\langle T'^2 \rangle$ ($\frac{V}{V_T}$ close to 1), it is reasonable to assume $W \approx W_T$. Together with Eqs. (19), (20), (B9), and (B11) we obtain Eq. (24):

$$\frac{\langle R_1'^2 \rangle}{\langle T'^2 \rangle} = \frac{\langle P'^2 \rangle}{\langle T'^2 \rangle} = \frac{V}{V_T} \approx \frac{3 + n^2\text{Da}_\theta + \text{Da}_\theta}{3 + n^2\text{Da}_\theta + 2\text{Da}_\theta}. \quad (\text{B12})$$

From Eqs. (A14)–(A16), the ratio between the fluctuation magnitudes of R_2 and R_1 is determined as

$$\frac{\langle R_2'^2 \rangle}{\langle R_1'^2 \rangle} = \frac{v}{V} \approx \frac{3 + 2\text{Da}_\theta}{3 + n^2\text{Da}_\theta + \text{Da}_\theta}, \quad (\text{B13})$$

which leads to Eq. (23) as

$$\frac{\langle R_2'^2 \rangle}{\langle T'^2 \rangle} = \frac{\langle R_1'^2 \rangle \langle R_2'^2 \rangle}{\langle T'^2 \rangle \langle R_1'^2 \rangle} = \frac{V}{V_T} \frac{v}{V} \approx \frac{3 + 2\text{Da}_\theta}{3 + n^2\text{Da}_\theta + 2\text{Da}_\theta}. \quad (\text{B14})$$

APPENDIX C: COHERENCY SPECTRUM

In the model system at study, characterized by weakly reacting scalars, R_1 and R_2 are sustained by fluctuations introduced by external sources (here randomly added in the Fourier space). We find numerically the two following results:

- (1) The energy spectra of R_1 and R_2 have the same shape.
- (2) The correlation coefficient between R_1 and R_2 conditional on a given wave vector is k independent.

These evidences allow to formulate a prediction on the shape of the coherency spectrum as follows. We consider here the one-dimensional case, and analysis in three-dimensional space can be implemented similarly. The fluctuating parts of R_1 and R_2 are expressed in the form of Fourier modes as

$$R_1' = \sum_k A_k(t) \sin(kx) + a_k(t) \cos(kx), \quad R_2' = \sum_k B_k(t) \sin(kx) + b_k(t) \cos(kx). \quad (\text{C1})$$

Their global correlation coefficient is

$$\begin{aligned} r(R_1, R_2) &= \frac{\langle [\sum_k A_k(t) \sin(kx) + a_k(t) \cos(kx)] [\sum_k B_k(t) \sin(kx) + b_k(t) \cos(kx)] \rangle}{\langle [\sum_k A_k(t) \sin(kx) + a_k(t) \cos(kx)]^2 \rangle^{1/2} \langle [\sum_k B_k(t) \sin(kx) + b_k(t) \cos(kx)]^2 \rangle^{1/2}} \\ &= \frac{\sum_k \overline{A_k B_k} + \overline{a_k b_k}}{[\sum_k (\overline{A_k^2} + \overline{a_k^2})]^{1/2} [\sum_k (\overline{B_k^2} + \overline{b_k^2})]^{1/2}}, \end{aligned} \quad (\text{C2})$$

where $\bar{\cdot}$ denotes time average.

Since the energy distributions of R_1 and R_2 on different length scales are the same (result 1), we define α as

$$\frac{\overline{A_1^2} + \overline{a_1^2}}{\overline{B_1^2} + \overline{b_1^2}} = \frac{\overline{A_2^2} + \overline{a_2^2}}{\overline{B_2^2} + \overline{b_2^2}} = \dots = \frac{\sum_k (\overline{A_k^2} + \overline{a_k^2})}{\sum_k (\overline{B_k^2} + \overline{b_k^2})} = \alpha^2.$$

Then the denominator of Eq. (C2) can be further written as

$$\begin{aligned} \left[\sum_k (\overline{A_k^2} + \overline{a_k^2}) \right]^{1/2} \left[\sum_k (\overline{B_k^2} + \overline{b_k^2}) \right]^{1/2} &= \left(\sum_k \overline{B_k^2} + \overline{b_k^2} \right) \alpha = \sum_k \alpha (\overline{B_k^2} + \overline{b_k^2}) \\ &= \sum_k (\overline{A_k^2} + \overline{a_k^2})^{1/2} (\overline{B_k^2} + \overline{b_k^2})^{1/2}. \end{aligned}$$

Thus it yields

$$r(R_1, R_2) = \frac{\sum_k \overline{A_k B_k} + \overline{a_k b_k}}{\sum_k (\overline{A_k^2} + \overline{a_k^2})^{1/2} (\overline{B_k^2} + \overline{b_k^2})^{1/2}}. \quad (\text{C3})$$

The coherency spectrum between R'_1 and R'_2 , Co_{R_1, R_2} , describes the correlation coefficients between two scalars corresponding to each length scale. At the mode k ,

$$\begin{aligned} \text{Co}_{R_1, R_2}(k) &= \frac{\langle [A_k(t) \sin(kx) + a_k(t) \cos(kx)][B_k(t) \sin(kx) + b_k(t) \cos(kx)] \rangle}{\langle [A_k(t) \sin(kx) + a_k(t) \cos(kx)]^2 \rangle^{1/2} \langle [B_k(t) \sin(kx) + b_k(t) \cos(kx)]^2 \rangle^{1/2}} \\ &= \frac{\overline{A_k B_k} + \overline{a_k b_k}}{(\overline{A_k^2} + \overline{a_k^2})^{1/2} (\overline{B_k^2} + \overline{b_k^2})^{1/2}}. \end{aligned} \quad (\text{C4})$$

According to result 2, the correlation coefficients at a given wave vector between R_1 and R_2 are independent of the wave vector; i.e.,

$$\frac{\overline{A_k B_k} + \overline{a_k b_k}}{(\overline{A_k^2} + \overline{a_k^2})^{1/2} (\overline{B_k^2} + \overline{b_k^2})^{1/2}} = \text{const} \quad \forall k. \quad (\text{C5})$$

By means of Eqs. (C4) and (C5), this gives

$$\text{Co}_{R_1, R_2}(k) = r(R_1, R_2) \quad \forall k. \quad (\text{C6})$$

Therefore, the global correlation coefficient between R_1 and R_2 is the same as the correlation coefficient at each wave number or length scale.

APPENDIX D: CORRELATION COEFFICIENT OF REACTIVE SCALAR GRADIENTS

As shown in Figs. 7 and 8, the energy distribution and the correlation coefficients of the reactive scalars remain almost independent of the length scale. Under these two conditions, we are ready to derive that the global correlation coefficient between two reactive scalars is the same as their coherency spectrum at each length scale (as seen in Appendix C).

Another quantity of primary importance is the global correlation coefficients of the gradients of scalars, which can be defined along one direction (e.g., x) only because of isotropy:

$$r(\theta_{1,x}, \theta_{2,x}) = \frac{\left\langle \frac{\partial \theta_1}{\partial x} \frac{\partial \theta_2}{\partial x} \right\rangle}{\left(\left\langle \left(\frac{\partial \theta_1}{\partial x} \right)^2 \right\rangle \right)^{1/2} \left(\left\langle \left(\frac{\partial \theta_2}{\partial x} \right)^2 \right\rangle \right)^{1/2}}. \quad (\text{D1})$$

For various scalars, the (almost) identical spectra of the scalar energy implies the (almost) identical spectra of the energy of scalar gradient quantities. In addition, since Eq. (29) is the definition of the coherency spectrum between not only θ_1 and θ_2 but also their gradients, the coherency spectra between the gradients of two reactive scalars are also almost k independent. Therefore, the correlation coefficient of the gradients of two reactive scalars is also identical at each length scale, and supposed to be the same as the correlation coefficient of these two reactive scalars. Figure 9 presents the global correlation coefficients of the reactive scalars and their gradients against Da with $\text{Re}_\lambda = 150$, $\text{Sc} = 1$, and $n = 1$. The speculation that the correlation coefficients between the reactive

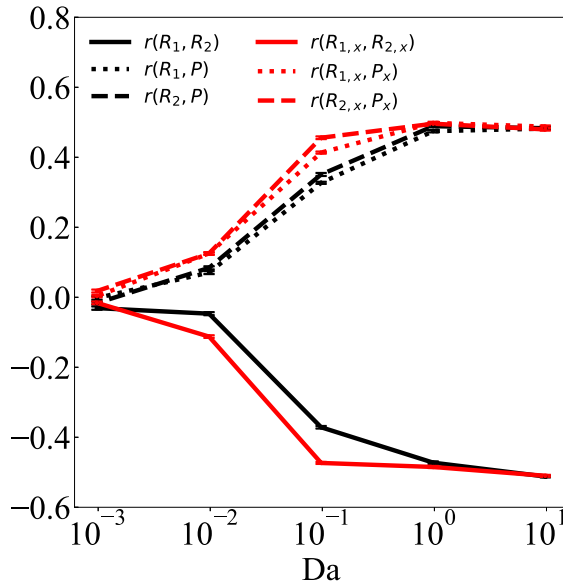


FIG. 9. The global correlation coefficients of the reactive scalars and their gradients along the x direction, under the condition of $Re_\lambda = 150$, $Sc = 1$, and $n = 1$.

scalars are the same as that of their gradients is well satisfied, except for the cases of $Da = 0.01$ and 0.1 , in which the condition that the coherency spectra is k independent is not satisfied at the largest scales (Fig. 8).

-
- [1] Z. Warhaft, Passive scalars in turbulent flows, *Annu. Rev. Fluid Mech.* **32**, 203 (2000).
 - [2] S. Corrsin, The reactant concentration spectrum in turbulent mixing with a first-order reaction, *J. Fluid Mech.* **11**, 407 (1961).
 - [3] Y. Pao, Statistical behavior of a turbulent multicomponent mixture with first-order reactions, *AIAA J.* **2**, 1550 (1964).
 - [4] E. E. O'Brien, Decaying second-order isothermal reaction in final period turbulence, *Phys. Fluids* **9**, 215 (1966).
 - [5] E. E. O'Brien, Very rapid, isothermal, two-species reactions in final period turbulence, *Phys. Fluids* **14**, 1804 (1971).
 - [6] R. G. Lamb and W. R. Shu, A model of second-order chemical reactions in turbulent fluid. I. Formulation and validation, *Atmos. Environ.* **12**, 1685 (1978).
 - [7] T. G. Heeb and R. S. Brodkey, Turbulent mixing with multiple second-order chemical reactions, *AIChE J.* **36**, 1457 (1990).
 - [8] H. L. Toor, Turbulent mixing of two species with and without chemical reactions, *Ind. Eng. Chem. Fundamen.* **8**, 655 (1969).
 - [9] L. Seuront, F. Schmitt, Y. Lagadeuc, D. Schertzer, S. Lovejoy, and S. Frontier, Multifractal analysis of phytoplankton biomass and temperature in the ocean, *Geophys. Res. Lett.* **23**, 3591 (1996).
 - [10] S. Lovejoy, W. J. S. Currie, Y. Tessier, M. R. Claereboudt, E. Bourget, J. C. Roff, and D. Schertzer, Universal multifractals and ocean patchiness: Phytoplankton, physical fields and coastal heterogeneity, *J. Plankton Res.* **23**, 117 (2001).
 - [11] J. Derot, F. G. Schmitt, V. Gentilhomme, and S. B. Zongo, Long-term high frequency phytoplankton dynamics, recorded from a coastal water autonomous measurement system in the eastern english channel, *Cont. Shelf Res.* **109**, 210 (2015).

- [12] J. Schumacher, K. R. Sreenivasan, and V. Yakhot, Asymptotic exponents from low-Reynolds-number flows, *New J. Phys.* **9**, 89 (2007).
- [13] K. Alvelius, Random forcing of three-dimensional homogeneous turbulence, *Phys. Fluids* **11**, 1880 (1999).
- [14] T. Gotoh, T. Watanabe, and Y. Suzuki, Universality and anisotropy in passive scalar fluctuations in turbulence with uniform mean gradient, *J. Turbul.* **12**, N48 (2011).
- [15] T. Gotoh and T. Watanabe, Power and Nonpower Laws of Passive Scalar Moments Convected by Isotropic Turbulence, *Phys. Rev. Lett.* **115**, 114502 (2015).
- [16] M. Gauding, L. Danaila, and E. Varea, High-order structure functions for passive scalar fed by a mean gradient, *Int. J. Heat Fluid Flow* **67**, 86 (2017).
- [17] M. Gauding, L. Danaila, and E. Varea, One-point and two-point statistics of homogeneous isotropic decaying turbulence with variable viscosity, *Int. J. Heat Fluid Flow* **72**, 143 (2018).
- [18] T. Y. Hou and R. Li, Computing nearly singular solutions using pseudo-spectral methods, *J. Comput. Phys.* **226**, 379 (2007).
- [19] J. R. Ristorcelli, Passive scalar mixing: Analytic study of time scale ratio, variance, and mix rate, *Phys. Fluids* **18**, 075101 (2006).
- [20] S. Corrsin, Simple theory of an idealized turbulent mixer, *AIChE J.* **3**, 329 (1957).
- [21] C. Bahri, G. Arwatz, W. K. George, M. E. Mueller, and M. Hultmark, Self-similarity of passive scalar flow in grid turbulence with a mean cross-stream gradient, *J. Fluid Mech.* **780**, 215 (2015).
- [22] S. Corrsin, The isotropic turbulent mixer: Part II. Arbitrary schmidt number, *AIChE J.* **10**, 870 (1964).
- [23] A. N. Kolmogorov, Local structure of turbulence in an incompressible fluid at very high Reynolds numbers, *Dokl. Akad. Nauk. SSSR* **30**, 299 (1941).
- [24] A. N. Kolmogorov, Energy dissipation in locally isotropic turbulence, *Dokl. Akad. Nauk. SSSR* **32**, 19 (1941).
- [25] J. Jimenez, Oceanic turbulence at millimeter scales, *Sci. Mar.* **61**, 47 (1997).